Theoretical study of an inviscid transonic flow near a discontinuity in wall curvature (Part 2)

Yumashev, Dmitry

2012

MIMS EPrint: **2012.39**

Manchester Institute for Mathematical Sciences
School of Mathematics

The University of Manchester

Reports available from: http://eprints.maths.manchester.ac.uk/
And by contacting: The MIMS Secretary
School of Mathematics
The University of Manchester
Manchester, M13 9PL, UK

ISSN 1749-9097

Theoretical study of an inviscid transonic flow near a discontinuity in wall curvature (Part 2)

DMITRY YUMASHEV[1]

[1]School of Mathematics, University of Manchester, Oxford Road, Manchester, M13 9PL, UK

(Received ?? and in revised form ??)

This work is Part 2 of the extensive theoretical study of an inviscid transonic flow near a discontinuity in wall curvature, focusing on the flow regimes with the *limiting characteristic*. The closed-form solutions obtained in Part 1 using the *hodograph method* are extended beyond the limiting characteristic by means of analytical continuation, and the results are analysed using the *phase portrait technique*. It is shown that if the flow can be extended beyond the limiting characteristic, it subsequently develops a shock wave. This leads to multiple solutions and a wider variety of flow regimes, including the ones with a concave downstream wall. As a consequence, a fundamental link between the local and the global flow patterns is observed in our problem.

Key Words:

1. Introduction

In Part 1 we considered an inviscid transonic flow in the vicinity of a curvature break (assuming the boundary-layer separation is local). This analysis revealed a complicated physical picture of the flow depending on the ratio of the curvatures. For example, we observed a certain type of supersonic flows which decelerate to subsonic speeds without a shock wave, transonic Prandtl–Meyer flow and supersonic flows with a weak shock. For most of the flow regimes it was possible to obtain a unique solution for the local flow given the ratio of the curvatures. In particular, it was demonstrated that the wall curvature discontinuity leads to the singular pressure gradients $\partial p/\partial x \sim G_{\mp}\,(\mp x)^{-1/3}$ upstream and downstream of the break, respectively, and the amplitude coefficients $G_{\mp}$ could be expressed as implicit analytical functions of the ratio of the curvatures. However, certain transonic flow regimes show a fundamentally different behaviour.

One of the central concepts of transonic aerodynamics is the *limiting characteristic*. It appears to be an important boundary between physically different regions of transonic flow with respect to a propagation of small perturbations (see for example Liepmann & Roshko 1957; Landau & Lifshitz 1959; Cole & Cook 1986). Thanks to this property, some low-speed supersonic flows which have not passed through the limiting characteristic yet can actually be decelerated to subsonic speeds without forming a shock wave. However, once a flow has passed through the limiting characteristic, it can only be decelerated to subsonic speeds by going though a shock. It turns out that extending the flow beyond the *limiting characteristic* is both the necessary and the sufficient condition of a shock formation.

In the present paper we apply the combination of the hodograph method and the phase

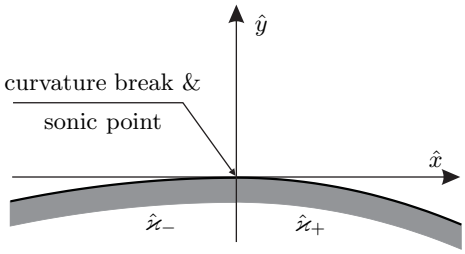

FIGURE 1. A discontinuity in wall curvature.

portrait technique to extend the analytical solutions from Part 1 beyond the limiting characteristic and prove these important results for our specific type of the flow. It is demonstrated that for the flow regimes with the limiting characteristic the pressure amplitudes $G_{\mp}$ have multiple solutions, each with two distinct branches for a weak and a strong shock, suggesting that the local flow with a shock gains an extra degree of freedom and becomes dependent on the global flow. This is because small perturbations ("information") cannot propagate upstream once the flow passes through the limiting characteristic. As a consequence, a fundamental link between the local and the global flow patterns is observed in our problem, and if the local flow with a shock is to be defined uniquely, one extra parameter (in addition to the ratio of the curvatures) needs to be specified.

2. Overview of the main definitions and results from Part 1

This section outlines the main definitions and results from Part 1 which are essential for the present analysis. The local surface shape close to a curvature break (Figure 1) is expressed as

$$y_w(x) = -\frac{\varkappa_\pm x^2}{2} + \dots, \qquad x \gtrless 0\,,$$

where $\varkappa_\pm$ stand for the wall curvatures, the dots represent higher-order terms in the coordinate expansions, and all the spacial variables (including the curvatures) have been scaled using either of the curvature radii (or their combination). In our definition $\varkappa_\pm > 0$ for convex walls.

To make sure the flow near the curvature discontinuity is transonic, we assume that the point $(x, y) = (0, 0)$ where the curvature breaks is also a *sonic point*. The velocity at this point is used to scale all the velocity components as well as the speed of sound. By restricting the analysis to isoenthalpic potential flows, the Euler equations can be reduced to the system containing only the velocity components $U = \partial\Phi/\partial x$, $V = \partial\Phi/\partial y$ and the local speed of sound a:

$$\left.\begin{aligned} &\big(a^2 - U^2\big)\frac{\partial U}{\partial x} + \big(a^2 - V^2\big)\frac{\partial V}{\partial y} = UV\left(\frac{\partial U}{\partial y} + \frac{\partial V}{\partial x}\right), \\ &\frac{U^2 + V^2}{2} + \frac{a^2}{\gamma - 1} = \frac{\gamma + 1}{2(\gamma - 1)}\,, \end{aligned}\right\} \tag{2.1}$$

where γ is the specific heat ratio.

System (2.1) is solved subject to the impermeability boundary condition upstream and downstream of the curvature discontinuity, which may be transferred to the $y = 0$ axis in the leading order, providing $|\varkappa_\pm\, x| \ll 1$:

$$V|_{y=0,\ x\gtrless 0} = -\varkappa_\pm\, x\,. \tag{2.2}$$

This automatically restricts our attention to the upper half-plane, $y \geqslant 0$. As one moves closer to the origin, no length scale can be assigned to the problem and the Euler equations are expected to admit self-similar solutions (Cole & Cook 1986); the scaled coordinates (x, y) can be used as small parameters to construct asymptotic expansions in this local region.

Introducing the similarity variable $\xi = x/y^\alpha$, where α is an unknown parameter which is to be determined, we construct asymptotic expansion of the velocity potential near the sonic point:

$$\Phi(x,y) = x + y^\sigma F(\xi)/(\gamma+1) + \dots, \qquad \sigma = \sigma(\alpha)\,, \quad y \to 0\,, \quad \xi = O(1)\,. \tag{2.3}$$

Substituting this expansion into (2.1) and using the principle of least degeneration results in the ODE (Frankl 1947):

$$\big[(\alpha\xi)^2 - F'\big]F'' - 5\alpha(\alpha-1)\,\xi F' + 3(3\alpha-2)(\alpha-1)\,F = 0\,, \tag{2.4}$$

and shows that $\sigma = 3\alpha - 2$. Since $y = 0$ corresponds to $\xi = \pm\infty$ depending on the sign of x, boundary condition (2.2) reduces to

$$\alpha\big[\lambda F - \xi F'\big]\big|_{\xi\to\pm\infty} \sim -(\gamma+1)\varkappa_\pm\ x\,y^{3-3\alpha}\big|_{y\to 0}\,, \qquad x \gtrless 0\,, \tag{2.5}$$

where $\lambda = \frac{\sigma}{\alpha} = 3 - \frac{2}{\alpha}$. It is easily seen from (2.5) that α has to satisfy the constraint $3\alpha - 3 = \alpha$, yielding $\alpha = 3/2$, $\lambda = 5/3$. Hence, (2.5) takes the form

$$\lim_{\xi\to\pm\infty}\left[\frac{\lambda F}{\xi} - F'\right] = -\frac{(\gamma+1)\varkappa_\pm}{\alpha}\,, \qquad x \gtrless 0\,. \tag{2.6}$$

The boundary-value problem (2.4), (2.6) can be studied both numerically and analytically.

Asymptotic analysis of (2.4) suggests that the pressure gradient on the walls upstream and downstream of the discontinuity develops a singularity:

$$\left.\frac{\partial p}{\partial x}\right|_{y=0,\,x\gtrless 0} = \mp\, k\, G_\pm\,(\pm\,x)^{-1/3} + \dots, \qquad k = \frac{10\big[(\gamma+1)\varkappa_-\big]^{2/3}}{9}\,. \tag{2.7}$$

One of the central goals of the study is to establish a link between the amplitude coefficients $G_\pm$ and the ratio of the curvatures, $\varkappa_+/\varkappa_-$.

It is easy to notice that equation (2.4) admits the invariant group transformation

$$\xi = A\,\overline{\xi}\,, \qquad F = A^3\,\overline{F}\,, \tag{2.8}$$

where $A > 0$ is a stretch coefficient, and the bar denotes transformed variables. This is equivalent to the coordinate and curvature transformation

$$x = B\,\overline{x}\,, \quad y = B\,\overline{y}\,, \qquad \varkappa_\pm = B^{-1}\,\overline{\varkappa}_\pm\,, \tag{2.9}$$

with $B = A^{1/(1-\alpha)}$. Boundary conditions (2.6) are also invariant with respect to the transformation when $\alpha = 3/2$ (Yumashev 2010). In order to make the solution independent on a choice of the group constant A, we shall introduce two new functions of ξ proportional to the leading order velocity perturbations u, v (Guderley 1957):

$$f(\xi) = \frac{F'}{\alpha^2\xi^2} \equiv \frac{(u/y)}{\alpha^2\xi^2}\,, \quad g(\xi) = \frac{\lambda F - \xi F'}{\alpha^2\xi^3} \equiv \frac{(v/x)}{\alpha^3\xi^2}\,. \tag{2.10a, b}$$

One can easily convert (2.4) to the following autonomous equation (Guderley 1957):

$$\frac{dg}{df} = \frac{3g + 2(\alpha-1)f^2 - 3\alpha fg}{2f + 3(\alpha-1)g - 2\alpha f^2}\,, \tag{2.11}$$

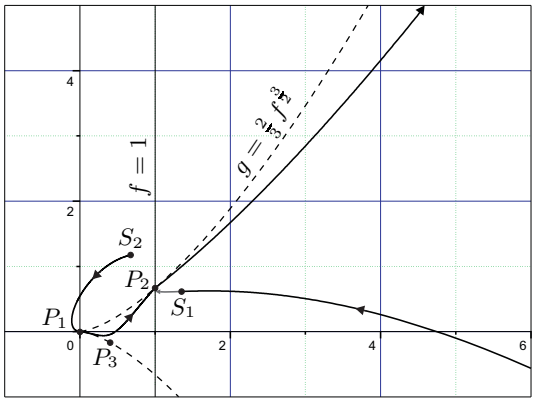

FIGURE 2. A typical phase trajectory which tunnels through the singular line $f = 1$ where the main equation (2.4) fails.

Now each solution of equation (2.4) may be treated as a phase trajectory in the (f, g) plane (this is usually referred to as the *phase portrait*). There are three critical points in the phase plane: nodes P_1, P_2 and saddle point P_3 (Figure 2). All of them have a profound physical meaning; the point $P_2 = (1, \frac{2}{3})$ is particularly important as it corresponds to the *limiting characteristic*. In this paper we shall focus on the phase trajectories that tunnel through P_2.

Our problem also admits a *momentum representation*, as opposed to the *coordinate representation* used so far (Chaplygin 1902). This implies treating the perturbations u, v of the velocity components as the independent variables, with the spatial coordinates being their functions: $x = x(u, v)$, $y = y(u, v)$. After inverting the roles of independent and dependent variables, the governing equations are transformed into the so-called Trikomi equations; these may be converted into a pair of linear second order equations for the functions $x(u, v)$ and $y(u, v)$ separately:

$$u\,\frac{\partial^2 y}{\partial v^2} - \frac{\partial^2 y}{\partial u^2} = 0\,, \quad u\,\frac{\partial^2 x}{\partial v^2} - \frac{\partial^2 x}{\partial u^2} + \frac{1}{u}\,\frac{\partial x}{\partial u} = 0\,. \tag{2.12a, b}$$

The transformation to system (2.12) is possible when the Jacobian

$$J_{uv} = \Big|\mathrm{Det}\begin{bmatrix} \partial x/\partial u & \partial y/\partial u \\ \partial x/\partial v & \partial y/\partial v \end{bmatrix}\Big| \neq 0\,. \tag{2.13}$$

If $J_{uv} = 0$ for certain solutions of (2.12), the corresponding functions $u(x, y)$ and $v(x, y)$ are many-valued and these solutions have no physical meaning (unless there is a shock wave). On the contrary, if $J_{uv} = \infty$ at some point, the functions $x(u, v)$, $y(u, v)$ are many-valued, suggesting that the same values of u, v occur in several different places within the flow, which is a normal situation.

The inverse problem described by (2.12) also admits a self-similar solution near the sonic point. Introducing the similarity variable $\zeta = u/v^\beta$, where β is an unknown parameter, we represent $x(u, v)$ and $y(u, v)$ in the form

$$x(u, v) = v\,\psi(\zeta) + \dots\,, \quad y(u, v) = u\,\varphi(\zeta) + \dots\,. \tag{2.14a, b}$$

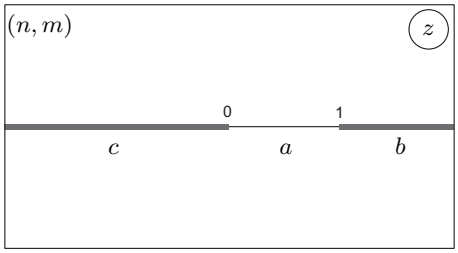

FIGURE 3. A sheet of the Riemann surface for the many-valued functions in (2.20); a, b, c mark the regions on the real axis which correspond to physically different flow regimes.

Substituting (2.14) into (2.12a), we get the following equation for $\varphi(\zeta)$:

$$\left(\beta^2\zeta^3 - 1\right)\varphi'' + \left(\beta(\beta+1)\zeta^2 - \frac{2}{\zeta}\right)\varphi' = 0\,, \qquad \varphi' = \frac{d\varphi}{d\zeta}\,.$$

This is a particular case of a *hypergeometric equation*. Transformation from ζ to a new variable z defined as (Cole & Cook 1986)

$$z = \left(1 - \beta^2\zeta^3\right)^{-1}\,, \tag{2.15}$$

yields

$$6z(1-z)\ddot{\varphi} + (3 - 11z)\dot{\varphi} = 0\,, \qquad \dot{\varphi} = \frac{d\varphi}{dz}\,. \tag{2.16}$$

The general solution of equation (2.16) can be expressed via an *incomplete beta function* $B(a, b, z)$ (see Abramovitz & Stegun 1972):

$$\varphi(z) = C_1 + C_2\, B\left(\tfrac{1}{2}, -\tfrac{1}{3}, z\right), \tag{2.17}$$

where C_1, C_2 are arbitrary constants. For the sake of simplicity we shall employ a shorter notation for the incomplete beta function from (2.17):

$$B(z) \equiv B\left(\tfrac{1}{2}, -\tfrac{1}{3}, z\right) = \int_0^z \frac{d\omega}{\omega^{1/2}(1-\omega)^{4/3}}\,. \tag{2.18}$$

The solution for $\psi(z)$ is readily expressed as

$$\psi(z) = C_3 + C_4\left[B(z) - 3z^{-1/2}(1-z)^{-1/3}\right]. \tag{2.19}$$

Out of the four integration constants only two are independent, resulting in the following general solution for x and y:

$$y = u\,\left[C_1 + C_2\, B(z)\right], \tag{2.20a}$$

$$x = v\,\left[C_1 + C_2\left(B(z) - 3z^{-1/2}(1-z)^{-1/3}\right)\right]. \tag{2.20b}$$

The functions $B(z)$ and $z^{1/2}(1-z)^{1/3}$ are defined on a 6-sheet Riemann surface, with the sheets joined via brunch-cuts $(-\infty, 0)$ (due to $z^{1/2}$) and $(1, \infty)$ (due to $(1-z)^{1/3}$), as shown in Figure 3. Each sheet is characterized by a pair of integer numbers (n, m) denoting brunches of the functions $z^{1/2}$ and $(1-z)^{1/3}$ accordingly, hence taking on the values $n = 1, 2$ and $m = 1, 2, 3$.

The phase variables are easily expressed in terms of the general solutions (2.20):

$$f(z) = \left(\frac{y/u}{x/v}\right)^2 \frac{z-1}{z} \equiv \left(\frac{\varphi(z)}{\psi(z)}\right)^2 \frac{z-1}{z}\,, \tag{2.21a}$$

$$g(z) = \beta \left(\frac{y/u}{x/v}\right)^3 \frac{z-1}{z} \equiv \beta \left(\frac{\varphi(z)}{\psi(z)}\right)^3 \frac{z-1}{z}\,, \tag{2.21b}$$

while the similarity variables ξ and ζ are related to one another through

$$\xi^2 = \frac{x^2}{y^3} \equiv \frac{(x/v)^2}{(y/u)^3}\,\frac{v^2}{u^3} = \frac{(x/v)^2}{(y/u)^3}\,\frac{1}{\zeta^3}\,, \tag{2.22}$$

The boundary conditions of the inverse problem are set at the points

$$z_- = \Big(1 - \beta^2\big(\lambda G_-\big)^3\Big)^{-1}\,, \quad z_+ = \Big(1 + \beta^2\big(\lambda G_+\big)^3 \big(\varkappa_-/\varkappa_+\big)^2\Big)^{-1}\,, \qquad z_\pm \in \mathbb{R}\,. \tag{2.23}$$

Satisfying the impermeability condition on the upstream wall (point z_- in the complex z plane) leads to the exact solutions

$$y = u\,\frac{z_-^{1/2}\big(1-z_-\big)^{1/3}}{3(\gamma+1)\varkappa_-}\,\Big[B(z) - B(z_-)\Big]\,, \tag{2.24a}$$

$$x = v\,\frac{z_-^{1/2}\big(1-z_-\big)^{1/3}}{3(\gamma+1)\varkappa_-}\,\left[B(z) - \frac{3}{z^{1/2}(1-z)^{1/3}} - B(z_-)\right]. \tag{2.24b}$$

Equations (2.24) are valid subject to an appropriate choice of branches for all the complex-valued functions, including $z_-^{1/2}$, $(1-z_-)^{1/3}$ and $B(z_-)$ (functions of the constant z_-), and this choice solely depends on the flow regime near the upstream wall. The main criterion is that x and y should always remain real.

Using the general solution (2.24) of the inverse problem, the Jacobian (2.13) may be expressed as

$$J_{uv} = \left|\frac{\partial(x,y)}{\partial(u,v)}\right| = -C^2\left[\left(\varphi - \frac{3z^{1/2}}{(1-z)^{1/3}}\right)^2 + 9(1-z)^{1/3}\right] \equiv z\,\left(\frac{x}{v}\right)^2\,(f-1)\,, \tag{2.25}$$

with $C = z_-^{1/2}\,(1-z_-)^{1/3}\,(3(\gamma+1)\varkappa_-)^{-1}$.

Even for the simplest flow regimes the trajectory in the z plane runs on at least two sheets of the Riemann surface, thus requiring to construct regular branches of all the many-valued functions in (2.24). To do this we shall use the standard exponential representation $z = r\,e^{i\vartheta}$ of a complex number z, with $-\pi < \vartheta < \pi$ on the sheets $(1,m)$ and $\pi < \vartheta < 3\pi$ on the sheets $(2,m)$. The values $\vartheta = 0,\,2\pi$ correspond to real positive $z \in (0,\infty)$. Similarly, $(1-z) = R\,e^{i\theta}$, with $-\pi < \theta < \pi$ on the sheets $(n,1)$, $\pi < \theta < 3\pi$ on the sheets $(n,2)$ and $3\pi < \theta < 5\pi$ on the sheets $(n,3)$. The values $\theta = 0,\,2\pi,\,4\pi$ correspond to real $z \in (-\infty,1)$. The arguments ϑ, θ have been chosen to run through when z moves from one sheet to another because this is convenient for describing transitions between the sheets; however, one can always use local arguments $\bar\vartheta$, $\bar\theta$ which are restricted within $(-\pi,\pi)$ on each sheet, thus giving the following expression for the regular branch of $z^{1/2}(1-z)^{1/3}$ on the sheet (n,m):

$$z^{1/2}(1-z)^{1/3} = r^{1/2}\,R^{1/3}\,\exp\left\{\frac{i\bar\vartheta}{2} + \frac{i\bar\theta}{3} + i\pi(n-1) + \frac{2\pi i}{3}(m-1)\right\}, \tag{2.26}$$

One of the flow regimes considered in Part 1 involves subsonic speeds on the upstream wall. For this regime the trajectory in the z plane, having started from point $r_- = |z_-| \in (0,1)$, was running on three sheets of the Riemann surface and ended at $r_+ = |z_+| > 1$. It was possible to continue solutions (2.24) analytically along the trajectory and satisfy

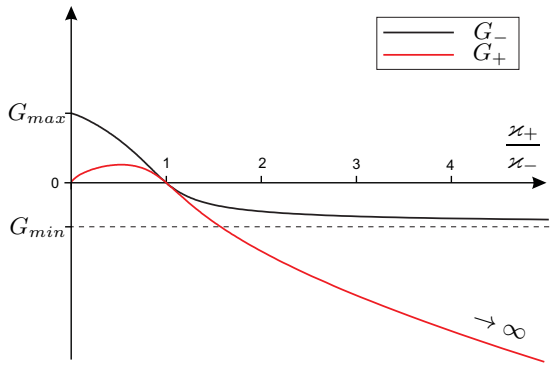

FIGURE 4. Upstream and downstream pressure gradients as functions of the ratio of the curvatures.

the second boundary condition at r_+ (downstream wall), yielding the algebraic system

$$B(r_-) = \frac{9\sqrt{\pi}\,\Gamma(2/3)}{\Gamma(1/6)} + I(r_+)\,, \tag{2.27a}$$

$$\frac{\varkappa_+}{\varkappa_-} = \frac{r_+^{1/2}\big(r_+ - 1\big)^{1/3}}{r_-^{1/2}\big(1 - r_-\big)^{1/3}}\,, \tag{2.27b}$$

where

$$I(r) = \int_r^\infty \frac{d\rho}{\rho^{1/2}(\rho-1)^{4/3}}\,, \qquad 1 < r < \infty\,.$$

These equations allow to determine any two of the three parameters r_-, r_+, $\varkappa_+/\varkappa_-$ for a given value of the third one. The most physically meaningful case is when the curvatures ratio $\varkappa_+/\varkappa_-$ is known and $r_\pm$ are expressed as functions of it, yielding (through (2.23)) the coefficients $G_\pm$ related to the wall pressure gradients; these solutions are plotted in Figure 4.

The other regimes considered in Part 1 involved the so-called *subcritical supersonic flow* on the upstream wall, which could be decelerated to subsonic speeds without a shock, and transonic Parndtl-Meyer flow. For all these regimes it was possible to use the closed-form solutions such as (2.27) to express the amplitude coefficients $G_\mp$ as implicit analytical functions of the ratio of the curvatures (Figure 4). However, one particular transonic flow regime shows a fundamentally different behaviour; it involves the so-called *supercritical supersonic flow* on the upstream wall, and also features the limiting characteristic and a weak shock, resulting in multiple solutions for the local flow. It is the main focus of the present paper.

3. Supercritical supersonic flow on the upstream wall

This regime takes place when phase trajectories start into the supercritical region (Figure 5), i.e. when $|g| < \frac{2}{3}\,f^{\frac{3}{2}}$, $G_- > G_{max} = 1/(\lambda\beta^{2/3})$, $\zeta_-^3 > \zeta_c^3$ and z_- is somewhere within the branch cut $(-\infty, 0)$ (Figure 3).

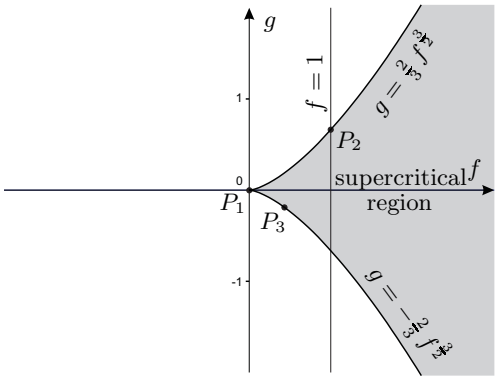

FIGURE 5. Supercritical region in the phase plane.

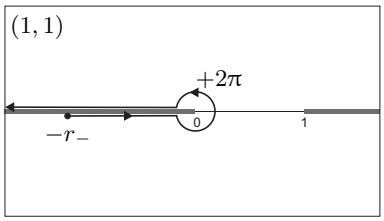

FIGURE 6. Initial fragment of the z plane trajectory corresponding to a supercritical supersonic flow near the upstream wall. Note that $z_- = -r_-$ in this case.

3.1. *Structure of the flow upstream of the limiting characteristic*

Without losing generality, we can continue solutions (2.24) analytically to the lower side of the branch cut on the sheet $(1,1)$ to get the following solution near the upstream wall:

$$y = u\,\frac{r_-^{1/2}\big(1+r_-\big)^{1/3}}{3(\gamma+1)\varkappa_-}\,\Big[J(r_-) - J(r)\Big]\,, \tag{3.1a}$$

$$x = v\,\frac{r_-^{1/2}\big(1+r_-\big)^{1/3}}{3(\gamma+1)\varkappa_-}\,\left[J(r_-) - J(r) - \frac{3}{r^{1/2}(1+r)^{1/3}}\right], \tag{3.1b}$$

where

$$J(r) = \int_0^r \frac{d\rho}{\rho^{1/2}(1+\rho)^{4/3}}\,.$$

Since $y \geqslant 0$ and $u > 0$ in the oncoming supersonic flow, $r \leqslant r_-$ in (3.1), and the z plane trajectory leaves to the right of z_-, travelling towards the origin (see Figure 6).

The subsequent behaviour of the z plane trajectory is obvious. Due to presence of the saddle point P_3 the relevant phase trajectory gradually turns upwards and crosses the line $g = 0$, i.e. the sign of v changes. This can be clearly seen from the computational results (section 2). Hence, in the z plane the trajectory reaches the point $z = 0$, and makes a single turnover along an infinitesimal circle around it, finding itself on the upper side of the supercritical branch cut $(-\infty, 0)$. The turnover transforms solutions (3.1) into

$$y = u\,\frac{r_-^{1/2}\big(1+r_-\big)^{1/3}}{3(\gamma+1)\varkappa_-}\,\Big[J(r_-) + J(r)\Big]\,, \tag{3.2a}$$

$$x = v\,\frac{r_-^{1/2}\big(1+r_-\big)^{1/3}}{3(\gamma+1)\varkappa_-}\left[J(r_-)+J(r)+\frac{3}{r^{1/2}(1+r)^{1/3}}\right]. \qquad (3.2b)$$

Now $v<0$, and x is still negative. The trajectory then moves from the origin to the left along the upper side of the branch cut, and runs towards $z=-\infty$ (see Figure 6). From solutions (3.2) and the general formulae (2.21) for the phase variables, one can easily obtain that $f\to 1$, $g\to\frac{2}{3}$ when $r\to\infty$. It means that the phase trajectory is moving towards the node $P_2=\big(1,\frac{2}{3}\big)$ located at the intersection of the upper critical line $g=\frac{2}{3}f^{\frac{3}{2}}$ and the singular line $f=1$ (Figure 2).†

To understand how the trajectories behave near the critical point P_2 and what happens after they have passed through this point, let us consider the asymptotic behaviour of (3.2) as $r\to\infty$. By introducing

$$C=\frac{r_-^{1/2}\big(1+r_-\big)^{1/3}}{3(\gamma+1)\varkappa_-}, \quad \sigma=J(r_-)+J(\infty), \qquad J(\infty)=\frac{3\sqrt{3\pi}\,\Gamma(2/3)}{\Gamma(1/6)}, \qquad (3.3)$$

we get:

$$\frac{y}{u}=C\sigma\left[1-\frac{6}{5\sigma}\,r^{-5/6}+\ldots\right], \quad \frac{x}{v}=C\sigma\left[1+\frac{9}{5\sigma}\,r^{-5/6}+\ldots\right], \qquad r\to\infty. \qquad (3.4)$$

It follows from these equations that

$$\xi^2=\frac{x^2}{y^3}=\frac{\beta^2}{C\sigma}\left[1+\frac{36}{5\,\sigma}\,r^{-5/6}+\ldots\right], \qquad r\to\infty. \qquad (3.5)$$

Therefore, $\xi\to\xi_c^-$ when $r\to\infty$, where

$$\xi_c=-\frac{\beta}{\big[J(r_-)+J(\infty)\big]^{1/2}}\left(\frac{3(\gamma+1)\varkappa_-}{r_-^{1/2}\big(1+r_-\big)^{1/3}}\right)^{1/2} \qquad (3.6)$$

refers to the position of the limiting characteristic in the physical plane.‡ Note that ξ_c may only be obtained if both $\varkappa_-$ and r_- (or $\varkappa_-$ and G_-) are known.

Plugging (3.4) into (2.21) yields the relevant asymptotic forms for the phase variables near P_2:

$$f=1-\frac{6}{\sigma}\,r^{-5/6}+r^{-1}+\ldots, \quad g=\beta\left[1+\frac{9}{\sigma}\,r^{-5/6}+r^{-1}+\ldots\right], \qquad r\to\infty. \qquad (3.7)$$

From these we can work out dg/df and d^2g/df^2 along the phase trajectories approaching P_2 from the left:

$$\frac{dg}{df}=1+\frac{\sigma}{15}\,r^{-1/6}+\ldots, \quad \frac{d^2g}{df^2}=-\frac{\sigma^2}{2\,(15)^2}\,r^{2/3}+\ldots, \qquad r\to\infty. \qquad (3.8)$$

Thus, the trajectories become tangent to the upper critical line when they reach the critical point, and the trajectories' curvature has a singularity at this point.¶ Hence, the function $g(f)$ is likely to have fractional powers of f in its expansion near P_2, making $f=1$ a branching point in the plane of complex f (the latter is obviously different from the phase plane). We now need to continue the solutions analytically through this point, so that they would remain real when $f>1$.

† Recall that P_2 is the only point where the phase trajectories are allowed to cross the singular line, and it corresponds to the limiting characteristic. See Part 1 for more details.

‡ In our case $\xi_c<0$ because $x<0$ in (3.2).

¶ One of the node's half lines also corresponds to $dg/df=1$, see Part 1.

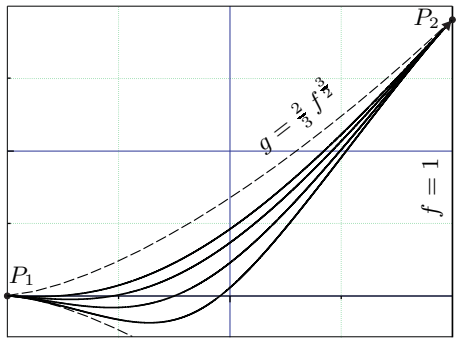

FIGURE 7. Supercritical phase trajectories before passing through the critical point P_2. The trajectories corresponding to larger values of G_- (stronger adverse pressure gradients on the upstream wall) are closer to the upper critical line $g = \frac{2}{3} f^{\frac{3}{2}}$.

3.2. *Extending the solutions beyond the limiting characteristic*

Let us perform the analytical continuation of the function $g(f)$ through the singular line via the point P_2. Equation (2.11) yields the following expansion of $\bar{g} = g - \frac{2}{3}$ over the powers of $\bar{f} = f - 1$:

$$\bar{g}(\bar{f}) = \bar{f}\left[G_1(\bar{f}) + (-\bar{f})^{\nu} G_2(\bar{f})\right], \qquad \bar{f} < 0\,, \quad |\bar{f}| \ll 1\,, \quad \nu = \frac{5\alpha - 7}{\alpha + 1}\,, \tag{3.9}$$

where the functions $G_1(\bar{f}) = 1 + a_1\,\bar{f} + a_2\,\bar{f}^{\,2} + ...$ and $G_2(\bar{f}) = b_0 + b_1\,\bar{f} + b_2\,\bar{f}^{\,2} + ...$ are analytical functions of their argument. It is clear that $\bar{f} = 0$ is a branching point in the complex plane $\bar{f}$ unless ν is an integer. Since $\nu = \frac{1}{5}$ when $\alpha = \frac{3}{2}$, the function $\bar{g}(\bar{f})$ has a total of 5 branches due to this point, defined on the relevant Riemann surface.

Writing the first two of terms of (3.9) explicitly gives

$$\bar{g}(\bar{f}) = \bar{f} + b_0\,(-\bar{f})^{6/5} + O\big(\bar{f}^{\,2}\big)\,.$$

The constant b_0 remains a free parameter upon substituting (3.9) into the equation (2.11) for the direct problem; analytical expression for b_0 can only be obtained from the inverse problem. Indeed, by plugging the last expression into the asymptotic expansions (3.8) we get the equation

$$\nu(\nu+1)b_0 = -\frac{(\sigma/15)^6}{2\left[(\nu+1)b_0\right]^4}\,,$$

which has the single real root †

$$b_0 = -\frac{1}{3}\left(\frac{\sigma}{6}\right)^{6/5}\,.$$

As expected, b_0 depends upon the value of r_- on the upstream wall (via σ). In other words, the phase trajectories corresponding to different upstream boundary conditions enter the point P_2 slightly differently, although $dg/df \to 1^+$ and $d^2g/df^2 \to -\infty$ when $f \to 1^-$ for all of them (Figure 7).

Expansion (3.9) is equivalent to the following asymptotic form of the function $F(\xi)$ as $\xi \to \xi_c^-$:

$$F(\xi) = F_c + F_c'\,(\xi - \xi_c) + \frac{F_c''}{2}\,(\xi - \xi_c)^2 + A\,(\xi_c - \xi)^{11/5} + ...\,; \tag{3.10}$$

† σ is defined in (3.3).

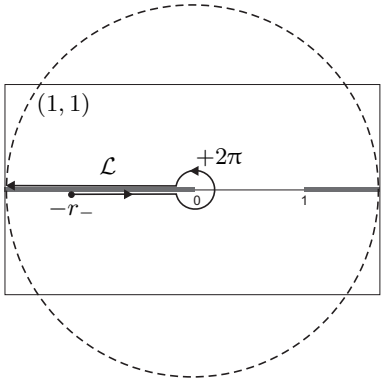

FIGURE 8. Analytical continuation of the solutions through the limiting characteristic is performed when the integration contour $\mathcal{L}$ moves to the infinite circle in the plane of complex z.

here

$$F_c = \frac{5\alpha^2\xi_c^3}{3\lambda}\,, \quad F_c' = \alpha^2\xi_c^2\,, \quad F_c'' = \alpha(\alpha-1)\xi_c\,, \quad A = \frac{15}{88}\,\frac{\xi_c}{|\xi_c|^{1/5}}\,\left(\frac{5\sigma}{18}\right)^{6/5}.$$

The fractional power term leads to a singularity in F''', causing singularities in the second derivatives of u, v. The function $(\xi-\xi_c)^{1/5}$ also has 5 branches defined on the relevant 5-sheet Riemann surface, and needs to be continued analytically to the right of ξ_c.

To perform the continuation, we are going to employ the general solutions (2.24) of the inverse problem, which take the form of (3.2) just before the phase trajectories reach the point P_2. For example, the first expression in (2.24) may be written as

$$\frac{y}{u} = \widetilde{C}\int_{\mathcal{L}} \frac{d\omega}{\omega^{1/2}(1-\omega)^{4/3}}\,, \qquad \widetilde{C} = \frac{z_-^{1/2}\big(1-z_-\big)^{1/3}}{3(\gamma+1)\varkappa_-}\,, \tag{3.11}$$

where the contour $\mathcal{L}$ (also called 'the z plane trajectory' in previous sections) is shown in Figure 8 and represents the supercritical supersonic upstream flow before passing through the limiting characteristic.† The regular branches of the functions $\omega^{1/2}(1-\omega)^{1/3}$, $z_-^{1/2}\big(1-z_-\big)^{1/3}$ are defined according to (2.26). Splitting the integral in (3.11) into two fragments along the lower and then the upper side of the branch cut $(-\infty,0)$ on the sheet $(1,1)$ ($n=m=1$, $\bar\theta=0$), and substituting $\bar\vartheta=\mp\pi$ respectively into (2.26), we obtain the regular branches of $\omega^{1/2}(1-\omega)^{1/3}$ on these sides. This immediately yields (3.2).

When $\mathcal{L}$ reaches $-\infty$, solution (3.11) is reduced to

$$\frac{y}{u} = C\Big[J(r_-)+J(\infty)\Big]\,, \qquad C = \widetilde{C}\,e^{i\pi/2} \equiv \frac{r_-^{1/2}\big(1+r_-\big)^{1/3}}{3(\gamma+1)\varkappa_-} \in \mathbb{R}\,.$$

Once at $-\infty$, the only possibility for the contour to move further is to join the infinite circle centred at the origin (Figure 8) and make several turnovers until the function $\omega^{1/2}(1-\omega)^{1/3}$ becomes real again on a different sheet of the Riemann surface. The minimal required change of $\arg z$ in these turnovers is simply equal to the least common multiple of 2 and 3 times π, thus giving $\Delta\arg z = 6\pi$ (three turnovers).

It can be easily shown that the three turnovers bring the z plane trajectory to the

† The contour starts at the point z_-, ends at any given point z (upper limit of the integral), and has to stay within the real axis everywhere in between.

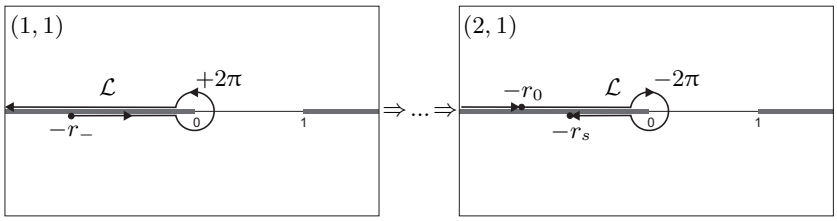

FIGURE 9. As a result of the analytical continuation describing how the flow passes through the limiting characteristic, the integration contour $\mathcal{L}$ in the z plane moves to another sheet of the Riemann surface.

upper side of the branch cut $(-\infty, 0)$ on the sheet $(2, 1)$ (Figure 9); as a result, the function $\omega^{1/2}(1-\omega)^{1/3}$ gains an extra multiple of $e^{i\pi} \equiv -1$. Now the contour has to move along the branch cut from $-\infty$ to the right as there is no other alternative of how to keep y real and ensure that the transformation $\xi(z)$ is monotonic. Since the integral along the infinite circle vanishes, solution (3.11) takes the form of

$$\frac{y}{u} = C\left[J(r_-) + J(\infty) - \int_\infty^r \frac{d\rho}{\rho^{1/2}(1+\rho)^{4/3}}\right] \equiv C\Big[J(r_-) + 2J(\infty) - J(r)\Big] \qquad (3.12)$$

after the transition. It is, in fact, the only non-trivial continuation of (3.2), as the next possible transition, characterized by $\Delta \arg z = 12\pi$, brings the trajectory back to where it started and yields (3.2); a transition with $\Delta \arg z = 18\pi$ results in (3.12), and so on.

Let us now find out what happens with the expansion (3.9) for $\bar{g}(\bar{f})$ when the z plane trajectory makes three turnovers along the infinite circle. From (3.7) it follows that $\bar{f} \sim z^{-5/6}$ when $z \to \infty$. Thus,

$$|\bar{f}| \to 0\,, \quad \Delta \arg \bar{f} = -\frac{5}{6}\,\Delta \arg z = -5\pi\,,$$

which means that $\Delta \arg(\bar{f}^{\,6/5}) = -6\pi$, transforming expansion (3.9) into

$$\bar{g}(\bar{f}) = \bar{f}\,\left[\,G_1(\bar{f}) + \bar{f}^{\,\nu}\,G_2(\bar{f})\,\right] = \bar{f} + b_0\,\bar{f}^{\,6/5} + O(\bar{f}^{\,2})\,, \qquad 0 < \bar{f} \ll 1\,.$$

As a result, the phase trajectories tunnel through P_2 to the right of the singular line, with $dg/df \to 1^-$ and $d^2g/df^2 \to -\infty$ when $\bar{f} \to 0^+$ (Figure 2). They literally get reflected from the upper critical line and stay within the supercritical region. The latter can also be seen from the fact that the z plane trajectory always remains on the branch cut $(-\infty, 0)$ unless a shock is developed (creating a jump in both the phase and the z plane trajectories – see section 3.3). Indeed, should it leave the branch cut for either the subsonic region $z \in (0, 1)$ or the subcritical supersonic region $z \in (1, \infty)$, solution (3.11) would become complex.

Based upon (3.12), we write the analytically continued solutions of the inverse problem in the form

$$y = C\,u\,\left[\,J(r_-) + 2J(\infty) - J(r)\,\right]\,, \qquad (3.13a)$$

$$x = C\,v\,\left[J(r_-) + 2J(\infty) - J(r) - \frac{3}{r^{1/2}(1+r)^{1/3}}\right]\,, \qquad (3.13b)$$

with the contour $\mathcal{L}$ running along the upper side of the branch cut $(-\infty, 0)$ on the sheet $(2, 1)$ from $-\infty$ towards the origin (Figure 9, right). These solutions express the flow immediately after passing through the limiting characteristic.

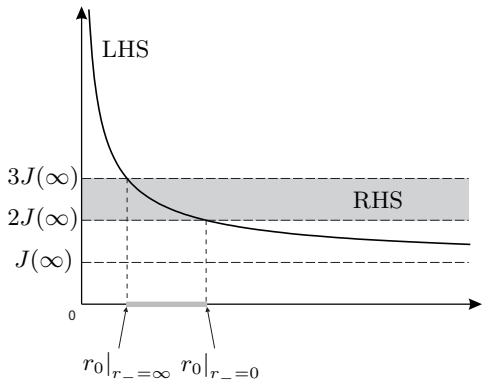

FIGURE 10. The left-hand side (LHS) of equation (3.14), plotted as a function of r_0, intersects with the shaded area representing all the possible values of the right-hand side (RHS) of (3.14). As a result, the solution for r_0 is confined within a finite interval.

3.3. *Shock formation*

It has already been observed in the computations that, after passing through the point P_2, the phase trajectory travels to (∞, ∞) and reflects in the $g = 0$ axis when x (and ξ) changes sign (Figure 2). This is exactly what solutions (3.13) give; rewriting them as

$$y/u = \frac{r_-^{1/2}\big(1+r_-\big)^{1/3}}{3(\gamma+1)\varkappa_-}\left[-J(r)+J(r_0)+\frac{3}{r_0^{1/2}\big(1+r_0\big)^{1/3}}\right],$$

$$x/v = \frac{r_-^{1/2}\big(1+r_-\big)^{1/3}}{3(\gamma+1)\varkappa_-}\left[-J(r)-\frac{3}{r^{1/2}(1+r)^{1/3}}+J(r_0)+\frac{3}{r_0^{1/2}\big(1+r_0\big)^{1/3}}\right],$$

where r_0 satisfies the equation

$$J(r_0)+3\,r_0^{-1/2}\big(1+r_0\big)^{-1/3} = J(r_-)+2J(\infty)\,, \tag{3.14}$$

we see that x, indeed, changes sign. This happens when the z plane trajectory passes through the point $z_0 = -r_0$ on the upper side of the branch cut $(-\infty, 0)$ (Figure 9, right). Since $u > 0$, $v < 0$ in the region considered, x is negative for $\infty > r > r_0$ and positive for $r_0 > r > 0$, in agreement with the requirement that $\xi(z)$ should grow monotonously along the contour $\mathcal{L}$. Equation (3.14) has a clear graphic solution which depends on the value of r_-, as shown in Figure 10. When r_- decreases from the infinity to zero, r_0 increases steadily and remains finite for all the values of r_-.

After passing through the point z_0, the z plane trajectory keeps moving towards the origin. Once in the origin, it makes a single turnover along an infinitesimal circle, funding itself on the lower side of the brunch cut (see Figure 9, right). Thus, v changes sign for the second time, as predicted in the computations, with the loci of streamlines minima at

$$\xi = \xi\big|_{v=0} = \frac{2}{\big[J(r_-)+2J(\infty)\big]^{\frac{3}{2}}}\left(\frac{3(\gamma+1)\varkappa_-}{r_-^{1/2}\big(1+r_-\big)^{1/3}}\right)^{1/2};$$

in comparison, the first change of sign of v corresponds to

$$\xi\big|_{v=0} = -\frac{2}{\left[J(r_-)\right]^{\frac{3}{2}}}\left(\frac{3(\gamma+1)\varkappa_-}{r_-^{1/2}\left(1+r_-\right)^{1/3}}\right)^{1/2}.$$

The relevant phase trajectory crosses the axis $g=0$, still remaining on the right of the singular line. In fact, the f-coordinate of the point where $g=0$ is given by

$$f\big|_{g=0} = \left[\frac{J(r_-)+2J(\infty)}{3}\right]^2 \geqslant \left[\frac{2J(\infty)}{3}\right]^2 \approx 2.231 > 1 \;\; \forall\, r_-\,.$$

As shown in the computations, the phase trajectory then moves towards the node point P_2, but never reaches it. Instead it tries to cross the singular line below P_2 (Figure 2). This behaviour can be explained theoretically. Indeed, after the turnover around the origin solutions (3.13) are transformed into

$$y/u = C\,\left[J(r)+J(r_-)+2J(\infty)\right]\,, \tag{3.15a}$$

$$x/v = C\,\left[J(r)+\frac{3}{r^{1/2}(1+r)^{1/3}}+J(r_-)+2J(\infty)\right]\,, \tag{3.15b}$$

with $u>0$, $v>0$ and $C = r_-^{1/2}\left(1+r_-\right)^{1/3}\left(3(\gamma+1)\varkappa_-\right)^{-1}$. The z plane trajectory now moves along the lower side of the supercritical branch cut to the left, so that r is increasing in (3.15). Plugging (3.15) into the expression (2.25) for the Jacobian and setting it to zero, we get the equation

$$\Big[J(r) - 3\,r^{1/2}(1+r)^{-1/3} + J(r_-) + 2J(\infty)\Big]^2 = 9\,(1+r)^{1/3}\,, \tag{3.16}$$

which again has a clear graphical solution at some finite point r_s, see Figure 11.† This is because the function

$$J(r) - 3r^{1/2}(1+r)^{-1/3}$$

decreases steadily from 0 to $-\infty$ with r; therefore, the left-hand side of (3.16) decreases from $\left[J(r_-)+2J(\infty)\right]^2$ to 0 (when the whole expression in the brackets becomes equal to zero) and then starts to grow again. On the way down it crosses the right-hand side of (3.16) which starts lower than the left-hand side at $r=0$ since $9 < \left[J(r_-)+2J(\infty)\right]^2$ for all r_-, but then monotonously grows with r.

After setting $r=r_s$ and performing a few trivial transformations, equation (3.16) can be rewritten as

$$J(r_s)+J(r_-)+2J(\infty) = \frac{3}{(1+r_s)^{1/3}}\left[r_s^{1/2}+\left(1+r_s\right)^{1/2}\right].$$

Solutions (3.15) then yield the following values of f and g when $r=r_s$:

$$f\big|_{r=r_s} = 1\,, \qquad g\big|_{r=r_s} = \frac{2}{3}\sqrt{\frac{r_s}{1+r_s}} < \frac{2}{3}\,. \tag{3.17}$$

Therefore, the trajectory is trying to pass through the singular line where it is not allowed to do so. This is illustrated in Figure 12 for the supercritical phase trajectories corresponding to different values of r_-. The only way to resolve this situation is to introduce a shock at a certain point $r_1 < r_s$ on the z plane trajectory, before the prohibited intersection with the singular line occurs.

† The graph is plotted in a logarithmic scale.

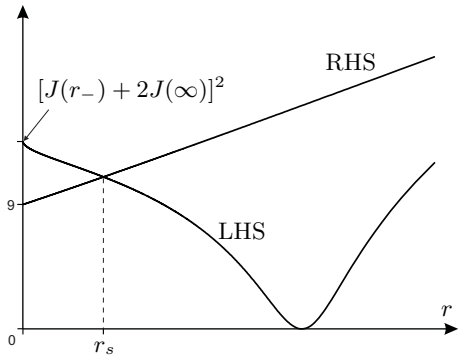

FIGURE 11. Left-hand side (LHS) and right-hand side (RHS) of equation (3.16) plotted as functions of r. The mutual intersection which takes place when $r = r_s$ corresponds to an illegitimate crossing of the singular line in the phase plane.

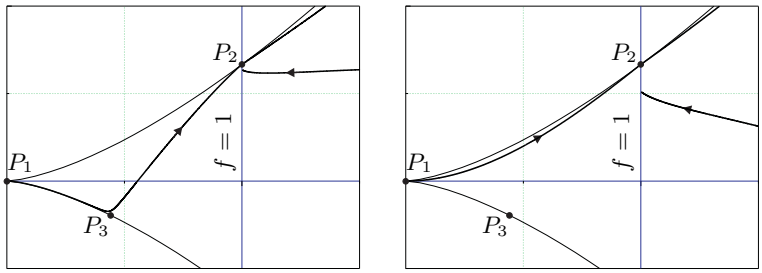

FIGURE 12. Supercritical phase trajectories corresponding to different values of r_-. After passing through the limiting characteristic (point P_2 on the singular line), the trajectories return to the singular line and tend to cross it below P_2.

The above results prove that *any oncoming supercritical supersonic flow necessarily leads to a shock formation*. Now one needs to perform a local analysis of the Hugoniot equations in order to continue the solutions through the shock. This was done in various works (see for example Cole & Cook 1986; Yumashev 2010), yielding the two conditions for the phase variables before and after the shock (subscripts 1 and 2, respectively):

$$f_1 + g_1 = f_2 + g_2 \tag{3.18a}$$

$$f_1 + f_2 = 2 \tag{3.18b}$$

It shows that the Hugoniot system, containing four equations (continuity equation, two momentum equations and energy equation), is degenerated into the system of only two equations when the asymptotic limit $x, y \ll 1$ is considered. System (3.18) describes the jump of the phase trajectories due to the shock; the second equation determines the shock strength and suggests that the points (f_1, g_1) and (f_2, g_2) are symmetric with respect to the singular line $f = 1$, whereas the first one provides the relevant change $g_2 - g_1$ of the vertical velocity component.

This result gives a basic understanding of how the supercritical supersonic flows behave. As opposed to the case of the subsonic and the subcritical supersonic flows, we shall assume that both of the parameters $\varkappa_-$ and G_- for the oncoming flow are known, therefore defining r_- uniquely according to (2.23) (provided that the upstream pressure gradient G_- is strong enough for the starting point z_- to be located in the supercrit-

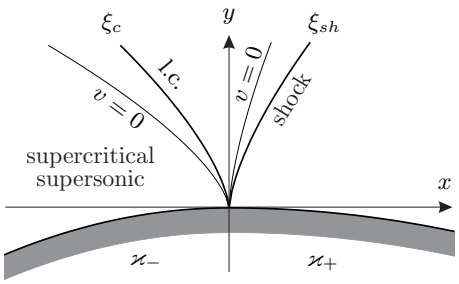

FIGURE 13. After passing through the limiting characteristic (l.c.), a supercritical supersonic flow inevitably develops a shock.

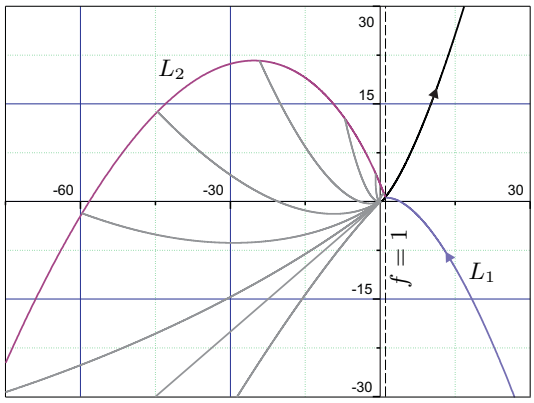

FIGURE 14. In the language of the phase variables, the upstream side of the shock may be located anywhere on the fragment L_1 of the phase trajectory coming from the upstream wall, while the downstream side of the shock lies somewhere on the curve L_2. The latter is the image of L_1 described by equations (3.18). The multiple trajectories that start on L_2 and return to the origin represent the flow between the shock and the downstream wall for different values of $\varkappa_+$; the lowermost of these trajectories does not intersect with L_2 and therefore has no physical meaning.

ical region, i.e. on the branch cut $(-\infty, 0)$). In this case solutions (3.1), (3.2), (3.13) and (3.15) allow to construct the relevant phase trajectory until the illegitimate crossing with the singular line (occurring at $z = -r_s$), and to determine the values of ξ along this trajectory (see equations (2.21), (2.22)). Theoretically the shock can form at any point of the final fragment L_1 of the phase trajectory with positive ξ (Figure 14). Note that we only consider shocks originated at the wall, which have $\xi_{sh} > 0$.† Thus, for any given supercritical pair of the parameters $\varkappa_-$ and G_-, the locus L_1 of the points (f_1, g_1) (possible locations of the left-hand side of the shock in the phase plane) is uniquely defined. Due to (3.18) this yields the corresponding locus L_2 of the points (f_2, g_2) (possible locations of the right-hand side of the shock in the phase plane), as shown in Figure 14. The latter has a clear maximum, and then goes down as $f_2, g_2 \to -\infty$.

The final fragment of the phase trajectory starts somewhere on L_2 and returns to the origin, but the available data ($\varkappa_-$, G_-) is insufficient for obtaining the exact position of this curve (Figure 14). Depending on the value of z_+, which is responsible for the

† The shocks induced by other sources and impinging upon the wall are located at $\xi_{sh} < 0$ and are excluded from the study.

asymptotic behaviour of the trajectory close to the origin, the last fragment may either be completely subsonic, partially or completely subcritical supersonic, or entirely supercritical supersonic. Hence, to get a unique solution one has to fix z_+ along with $\varkappa_-$, G_-, therefore leading to the *fundamental difference* between the supercritical flows and all other flows. Recall that for the oncoming subsonic (and also the subcritical supersonic flows) it was sufficient to set any two of the four parameters $\{\varkappa_-, r_-, \varkappa_+, r_+\}$, or $\{\varkappa_-, G_-, \varkappa_+, G_+\}$, in order to get the remaining two from (2.27). Now we need to fix any three parameters from these sets, say $\{\varkappa_-, r_-, r_+\}$, to find the forth one (in this case $\varkappa_+$). In other words, passing through the limiting characteristic (which inevitably leads to the shock formation) gives *one extra degree of freedom* to the supercritical supersonic flows. The local solution cannot be constructed based upon $\varkappa_\pm$ only (as it was clearly the case for the subsonic and the subcritical supersonic regimes), and requires one parameter from the global solution, be it a value of the pressure gradient on the upstream wall or a location of the shock.

When r_- and r_+ are specified, the phase trajectory can be constructed uniquely. If, in addition, $\varkappa_-$ is known, the relevant value of $\varkappa_+$ can be obtained from an obvious condition that ξ should be continuous at the shock. Indeed, the curvatures drop out of the expressions (2.21) for the phase variables, and therefore do not affect the phase trajectory. However, they are present in formula (2.22) which provides the values of ξ along the trajectory. It means that knowing r_-, r_+, together with the shock conditions (3.18), is sufficient for reconstructing both fragments of the phase trajectory (before and after the shock), whereas the values of ξ along these fragments depend upon $\varkappa_-$ before the shock and upon $\varkappa_+$ after the shock respectively. Thus, the continuity condition $\xi_1 = \xi_2 \equiv \xi_{sh}$ at the shock provides the required link between the curvatures.

3.4. *Structure of the flow behind the shock*

A detailed analysis of all the possible flow regimes behind the shock was performed by Yumashev (2010), and we are only going to list the key points here. Since ξ monotonously increases from 0 along L_1, it also increases along L_2 when moving from the left to the right (Figure 14), due to the continuity of ξ at the shock. The increase of ξ_{sh} means that the shock becomes more inclined, and its intensity drops (this can also be seen from the decrease of the parameter $H = f_1 - 1 = 1 - f_2$ while moving along L_2 to the right). Based on this observation, there is a total of six regimes which occur as ξ_{sh} keeps increasing, including the ones with a concave downstream wall ($\varkappa_+ < 0$):

(*a*) A subsonic flow immediately behind the shock, transforming into a subcritical supersonic flow on the downstream wall with $\varkappa_+ > 0$;

(*b*) An entirely subsonic flow between the shock and the downstream wall with $\varkappa_+ > 0$;

(*c*) A subsonic flow on the downstream wall with $\varkappa_+ < 0$;

(*d*) A subcritical supersonic flow between the shock and the downstream wall with $\varkappa_+ < 0$;

(*e*) A supercritical supersonic flow between the shock and the downstream wall with $\varkappa_+ < 0$;

(*f*) A supercritical supersonic flow between the shock and the downstream wall with $\varkappa_+ > 0$.

The ratio of the curvatures $\overline{\varkappa}_+ = \varkappa_+/\varkappa_-$ is plotted for all the regimes versus the scaled shock position $\overline{\xi}_{sh} = \frac{\xi_{sh}}{\sqrt{\varkappa_-}}$ in Figure 15, left, for all the possible flow regimes behind the shock. The curve, which appears to be invariant with respect to transformation (2.9), corresponds to one particular value of r_- (or G_-); one can plot a family of such curves for different r_-, and they would all look similar, simply being stretched along both axes

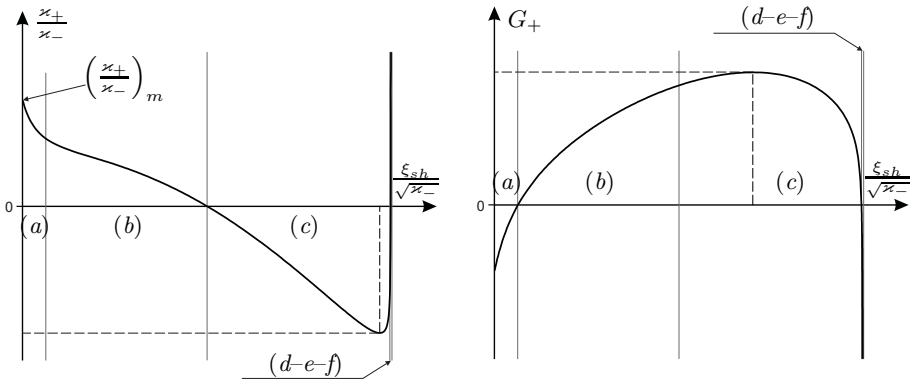

FIGURE 15. Connection between the relative location of the shock ($\frac{\xi_{sh}}{\sqrt{\varkappa_-}}$) and the downstream parameters $\frac{\varkappa_+}{\varkappa_-}$, G_+. The letters denote physically different regimes for a flow behind the shock. The graphs are plotted for a fixed value of the supercritical upstream pressure gradient G_-, and are invariant with respect to re-scaling of the spatial coordinates.

in a certain way. We see that within the regimes (a), (b) $\overline{\varkappa}_+$ decreases steadily with $\overline{\xi}_{sh}$ and becomes negative (concave downstream wall). The maximal possible ratio of the curvatures at $\xi_{sh} = 0$ corresponds to the critical angle beyond which the inviscid flow behind the shock separates from the downstream wall (Liepmann & Roshko 1957); it is equal to

$$\left(\frac{\varkappa_+}{\varkappa_-}\right)_{max} = \frac{r_m^{1/2}\left(r_m-1\right)^{1/3}}{r_-^{1/2}\left(1+r_-\right)^{1/3}}\,\frac{r_0^{1/2}\left(1+r_0\right)^{1/3}}{r_{00}^{1/2}\left(1-r_{00}\right)^{1/3}}\,, \tag{3.19}$$

where r_m is the only root of the equation

$$I(r_m) = \frac{3}{r_{00}^{1/2}\left(1-r_{00}\right)^{1/3}} - B(r_{00}) - \frac{9\sqrt{\pi}\,\Gamma(2/3)}{\Gamma(1/6)}\,, \qquad r_m > 1\,, \tag{3.20}$$

and

$$r_{00} = \frac{r_0}{1+2r_0} \tag{3.21}$$

(r_0 is defined in (3.14) for a given r_-).

The function $\overline{\varkappa}_+(\overline{\xi}_{sh})$ has a distinct minimum, therefore providing two different shock locations for any given curvatures' ratio: a strong shock ($\overline{\xi}_{sh} < \overline{\xi}_{min}$) and a weak shock ($\overline{\xi}_{sh} > \overline{\xi}_{min}$).† It is also clearly seen from Figure 15 that $\overline{\xi}_{sh}$ does not exceed a certain maximum value $\overline{\xi}_{max}$, the latter obviously corresponding to the degeneration of a weak shock into a characteristic of a supersonic flow (Liepmann & Roshko 1957).

As ξ_{sh} keeps increasing within regime (c), firstly the downstream wall pressure gradient reaches its maximum and starts decreasing (remaining adverse throughout), and secondly the ratio of the curvatures, now being negative, reaches its minimum and starts increasing. The latter yields the largest possible value of $|\varkappa_+/\varkappa_-|$ for a concave downstream wall ($\varkappa_+ < 0$) at which the attached shock can exist, and creates a demarcation line between the strong and the weak solutions for the shock.‡ This also provides an explanation for the well known experimental result that for a supersonic flow above a flat plate which

† The regimes (d), (e) and (f) could not be shown in Figure 15 and require a zooming.

‡ However, the value $(\varkappa_+/\varkappa_-)_{min}$ and the corresponding shock location ξ_{min} cannot be obtained analytically.

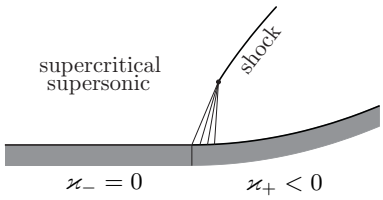

FIGURE 16. Detachment of the shock from the surface caused by a concave downstream wall (in this illustration $\varkappa_+/\varkappa_- = -\infty$).

turns into a concave wall the shock is always detached (see Figure 16). Indeed, in this case $\varkappa_+/\varkappa_- = -\infty$, whilst the largest possible value of $|\varkappa_+/\varkappa_-|$ resulting in the attached shock is finite.

The pressure gradient on the downstream wall G_+ is plotted in Figure 15, right, as a function of $\overline{\xi}_{sh}$ for all the regimes behind the shock. Again, the curve shown in Figure 15 corresponds to one particular value of G_-, which is due to the fact that supercritical flows have one extra degree of freedom. The downstream wall pressure gradient can be both favourable and adverse, depending on the flow regime.

When the shock inclination approaches the largest possible value $\left(\overline{\xi}_{sh}\right)_{max}$ (for a given upstream pressure gradient G_-), $\varkappa_+/\varkappa_-$ tends to ∞ (see Figure 15, left), and the the downstream pressure gradient G_+ has the following asymptotic behaviour (Figure 15, right):

$$G_+ \sim -\frac{1}{\lambda\beta^{2/3}}\left(\frac{\varkappa_+}{\varkappa_-}\right)^{2/3} \to -\infty \tag{3.22}$$

Equation (3.22) does not contain G_- (or r_-), suggesting that in the limit $\varkappa_+/\varkappa_- \to \infty$ the flow near the downstream wall depends only upon the curvatures' ratio. In other words, the additional degree of freedom, typical for the supercritical flows, vanishes, which makes the supercritical flow behave like the subcritical.

In this limiting case of $\varkappa_+/\varkappa_- \to \infty$ the phase trajectory moves towards the saddle point P_3 along its first asymptote. It means that the flow asymptotically becomes the Prandtl–Meyer flow as the downstream wall with $\varkappa_+ \to \infty$ is approached (assuming $\varkappa_- = O(1)$), thus being the only case when the phase trajectory does not return to the origin. However, the domain of the applicability of the above solutions in the physical plane is being degenerated to a point, and we need to perform a re-scaling. Indeed, since the problem is invariant with respect to transformation (2.9), the above limiting case may be treated as $\varkappa_- \to 0$ for $\varkappa_+ = O(1)$. It can be shown that this re-normalization leads to a uniform flow with $u = v = 0$ above the upstream wall with $\varkappa_- \to 0$, and the three coordinate lines where $v = 0$, as well as the limiting characteristic (ξ_c) and the shock (ξ_{sh}), all tighten to the vertical axis $x = 0$. The shock itself degenerates to a weak discontinuity located at $x = 0$, whereas the flow in region $x > 0$ corresponds to the phase trajectory running along the lower critical line $g = -\frac{2}{3}f^{\frac{3}{2}}$ from the saddle point to the origin. This regime has already been considered previously in Part 1, but at that time it appeared as the limiting case for the oncoming subsonic flow (when $\varkappa_- \to 0$).

We have just derived a fundamental property linking all the transonic flows near the curvature-break point, which is illustrated in Figure 17. The oncoming subsonic flows (for which $\varkappa_+/\varkappa_- > 1$) are succeeded by the subcritical supersonic flows, with the special case $\varkappa_- = \varkappa_+$ in between. The subcritical supersonic flows upstream, taking place for $0 < \varkappa_+/\varkappa_- < 1$, are succeeded by the supercritical supersonic flows when $\varkappa_+ \to 0$. As it was shown in sections 3.1–3.3, the supercritical regimes are physically different from all other

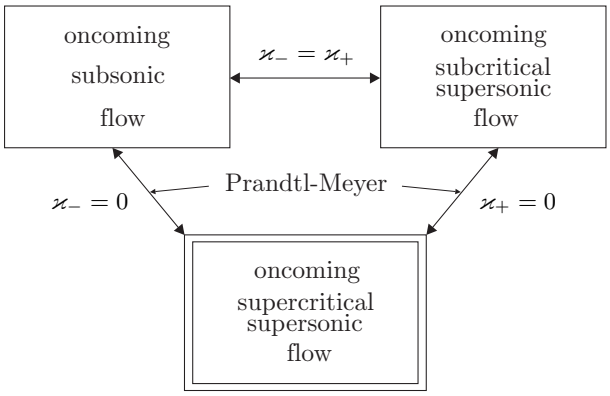

FIGURE 17. Links between all the possible transonic flow regimes near a discontinuity in wall curvature.

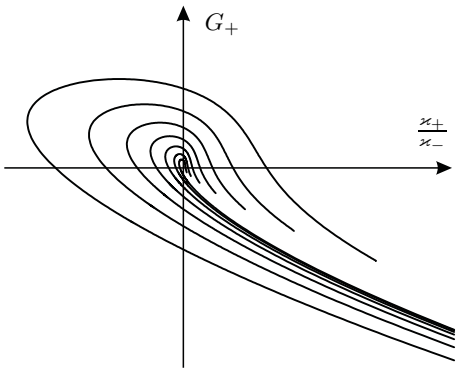

FIGURE 18. A family of the curves representing the downstream pressure gradient as a function of the curvatures' ratio in the supercritical regime. The curves are plotted for different values of the supercritical upstream pressure gradient G_-; wider curves correspond to larger values of G_-.

regimes because they require one extra parameter in order to determine the local flow pattern. In the limiting case $\varkappa_+ \to 0$ the supercritical flow pattern is completely different from the one obtained for the similar limit in the subcritical flows. Therefore, the local flow parameters (in particular the downstream wall pressure gradient) show a bifurcation-like behaviour at the turn of the subcritical and the supercritical supersonic regimes. The supercritical regimes also allow the solutions with $\varkappa_+ < 0$ (concave downstream walls), and are linked with the subsonic regimes via the limiting case $\varkappa_- \to 0$.† Therefore, we have a sequence of the possible regimes transforming from one into another, depending on the values of the basic input parameters (for example, $\varkappa_-$ and G_-).

† In this limiting case one extra degree of freedom degenerates, since the (physical) downstream pressure gradient $\partial p/\partial x$, according to (3.22) and (2.7), is finite and proportional to $\varkappa_+^{2/3}$ only. Although G_- still remains a free parameter in the supercritical solutions, the latter are reduced to a uniform flow upstream and the Prandtl–Meyer flow downstream of the curvature break. It can also be seen from (2.7) that the (physical) upstream pressure gradient is proportional to $G_-\varkappa_-^{2/3}$, and it vanishes with $\varkappa_-$ regardless of the value of G_-.

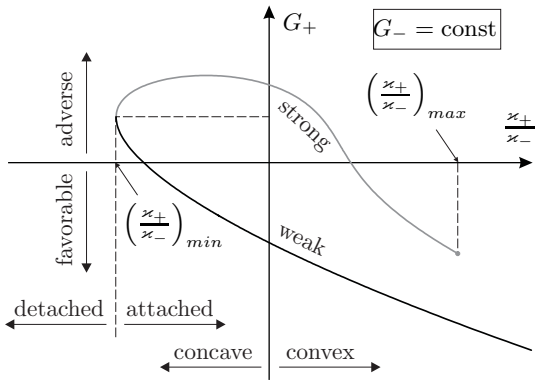

FIGURE 19. Physical interpretation for different fragments of a typical supercritical curve describing the downstream pressure gradient.

Finally, let us summarize the results obtained for the supercritical flows by plotting the downstream wall pressure gradient G_+ (Figure 18) versus the curvatures' ratio for different values of G_- (or r_-). As opposed to the subcritical regimes, now we have a family of the curves, which is due to the presence of one extra degree of freedom in the supercritical flows (for the subsonic and the subcritical supersonic flows there was only one such curve; see Part 1 for details). All the curves in Figure 18 have the same asymptotic behaviour when $\varkappa_+/\varkappa_- \to \infty$, in accordance with (3.22); they match with the appropriate curve for G_+ in subsonic regimes, therefore providing a link between the supercritical supersonic and the subsonic regimes discussed above. The clearly observed pair of the solutions for the pressure gradient within certain values of $\varkappa_+/\varkappa_-$ corresponds to the strong and the weak shocks (Figure 19). However, the strong solution seems to be physically unreasonable for our particular problem because it leads to

$$\frac{d\overline{\xi}_{sh}}{d\overline{\varkappa}_+} < 0\,, \qquad \overline{\xi}_{sh} = \frac{\xi_{sh}}{\sqrt{\varkappa_-}}\,, \qquad \overline{\varkappa}_+ = \frac{\varkappa_+}{\varkappa_-}\,,$$

and might be linked to a flow with an impinging shock. Moreover, it is the weak solution that yields the important limiting case $\varkappa_+/\varkappa_- \to \infty$, bringing the whole pattern back to the subsonic flows. On the weak branch in Figure 19 the downstream pressure gradient monotonously decreases with $\overline{\varkappa}_+$, and can be either adverse (for the most negative values of $\overline{\varkappa}_+$, close to the shock detachment from the wall) or favourable (for all other values of $\overline{\varkappa}_+$).

Both the subcritical and the supercritical solutions for the coefficients $G_\pm$ are plotted in Figure 20 as functions of the curvatures' ratio. This plot completes our study of the inviscid flow generated by a discontinuity in wall curvature.

4. Conclusions

We have considered an inviscid transonic flow in the vicinity of a curvature break (assuming the boundary-layer separation is local). This analysis revealed a complicated physical picture of the flow depending on the ratio of the curvatures, including the ones with a weak shock. Based on the results from Part 1, in this paper we focused on the flows that pass through the *limiting characteristic* (these flows are referred to as *supercritical*). The analytical solutions obtained using the hodograph method were extended beyond the limiting characteristic, which allowed to study all the downstream flow regimes in

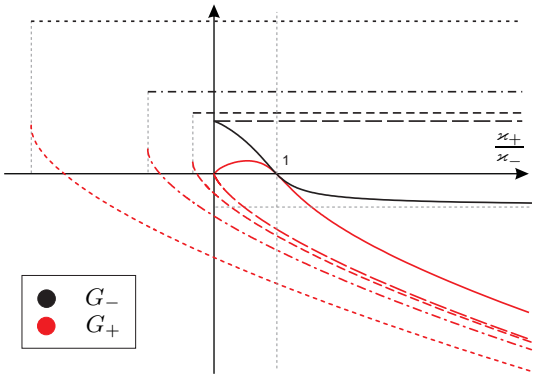

FIGURE 20. The pressure gradients $G_\pm$ plotted as functions of the curvatures' ratio for subcritical regimes (solid lines) and supercritical regimes (dashed lines). The non-uniqueness in the supercritical solution is due to an extra degree of freedom gained after passing through the limiting characteristic.

great detail. It turns out that the extension beyond the limiting characteristic inevitably leads to a shock formation. This leads to multiple solutions and a wider variety of flow regimes, including the ones with a concave downstream wall; in particular, it was demonstrated that for the supercritical flow regimes the pressure amplitudes $G_\mp$ have multiple solutions, each with two distinct branches for a weak and a strong shock. As a consequence, a fundamental link between the local and the global flow patterns is observed in our problem, and if the local flow with a shock is to be defined uniquely, one extra parameter (in addition to the ratio of the curvatures) needs to be specified.

The study was performed in 2007 as part of a PhD research project supported by the ORS Awards Scheme and the School of Mathematics, University of Manchester.

REFERENCES

ABRAMOVITZ, M & STEGUN, I A 1972 *Handbook Of Mathematical Functions With Formulas, Graphs, And Mathematical Tables*, 9th edn. Wiley-Interscience.

CHAPLYGIN, S 1902 Gas Jets. *Scientific Memoirs, Moscow University* .

COLE, J D & COOK, L P 1986 *Transonic Aerodynamics*. Elsevier Science Publishers B.V.

FRANKL, F I 1947 Studies in the theory of infinite aspect ratio wing moving with the speed of sound. *Dokl. Akad. Nauk SSSR* **57** (7), 1561–1564.

GUDERLEY, G 1957 *Theorie Schallnahe Stromungen.*. Springer-Verlag Berlin, english translation: Addison-Wesley 1962.

LANDAU, L D & LIFSHITZ, E M 1959 *Fluid Mechanics.*. Pergamon Press.

LIEPMANN, H W & ROSHKO, A 1957 *Elements of Gasdynamics.*. John Wiley & sons, New York.

YUMASHEV, D. 2010 Viscous-inviscid interaction in a transonic flow caused by a discontinuity in wall curvature. PhD thesis, University of Manchester.